

# Establishing Exciton Tunability in Two-Dimensional Perovskites

Kameron Hansen, October 2021

## Introduction

With the advent of epitaxial deposition techniques, quantum well structures based on III-V semiconductors such were first fabricated in 1970s. Strong confinement effects within the quantum wells allowed for stable excitons, i.e. bound electron-hole pairs that are responsible for light absorption, emission, and charge transport and therefore are at the center of the quantum well's optoelectronic properties. The properties of stable excitons in these quantum wells were investigated in the 1980s and 1990s, leading to a Nobel prize and the development of LEDs, electro-optic modulators, lasers, and photodetectors which are still considered state-of-the-art.<sup>1,2</sup>

Today, research efforts are focused on a new class of quantum well materials with stable excitons, namely two-dimensional metal halide perovskites (2D MHPs), which may be superior to III-V quantum wells for a variety of light-harvesting and light-emitting applications.<sup>3-6</sup> Unlike III-V quantum wells, 2D MHPs naturally crystallize into their  $A_2BX_4$  structure (shown in **Fig. 1**). This fundamental difference in the method of crystal growth has both advantages and disadvantages. On the one hand, the solution-based growth of 2D MHP crystals near room temperature is far more cost-effective and eco-friendlier than expensive epitaxial techniques. On the other hand, it was precisely the high level of control and tunability offered by epitaxial deposition which enabled the development of III-V quantum well technologies. Indeed, the success of these technologies is greatly attributed to advances in epitaxial methods that allowed for high tunability of the quantum well layer thicknesses, composition, and orientation, and crystalline quality.<sup>7-9</sup> Researchers leveraged these variables to tune the exciton properties and create optimized devices.

While this pathway towards developing exciton tunability is unavailable for 2D MHPs, nature has instead offered an alternative route through the wide catalog of molecules and atoms that naturally crystallize in the  $A_2BX_4$  structure. Indeed, over 50 different cations have successfully been incorporated into the A-site.<sup>6</sup> The B-site metal atom can vary between lead, tin, and germanium while the X-site halide is commonly occupied by iodide, bromide, or chloride. While a wide range of chemical compounds have been synthesized and incorporated into device structures, there is a lack of understanding as to how chemical substitutions within the  $A_2BX_4$  formula affect the material's exciton properties such as the binding energy, mass, diffusion length, lifetime, radius, dipole moment, and polarizability. Unfortunately, the same lattice effects (e.g. dynamic disorder and phonon-coupling) which give excitons in 2D MHPs their unique character and defect-tolerant properties also result in spectral structures which are difficult to interpret, and as a result, measurements of the exciton's properties are challenging.<sup>10</sup> Nowhere is this more evident than with the difficulty in measuring exciton binding energies ( $E_B$ ), a parameter of great importance for solar cell engineering as it determines the ratio of excitons to free carriers and for LED engineering as it strongly dictates electroluminescence quantum efficiency.<sup>11</sup> For example, taking the well-known 2D MHPs phenethylammonium lead iodide ( $PEA_2PbI_4$ ) and butylammonium lead iodide ( $BA_2PbI_4$ ) as case studies, state-of-the-art techniques for measuring  $E_B$  in 2D MHPs, namely absorption, photoluminescence excitation, electroabsorption, and low- and high-field magnetoabsorption at liquid helium temperatures have thus far led to  $E_B$  values ranging from 190 to 490 meV.<sup>12,13</sup> While some of this variance is caused by differences in the organic molecule, sample thickness, dielectric environment, and morphology, a significant portion of the variance originates from differing interpretations of band-edge absorption features and assumptions that are intrinsic to the measurement techniques. For theoretical and applied progress to continue forward, it is critical develop measurement techniques that are accurate and reproducible in determining the exciton's properties. Until the measurement uncertainty of  $E_B$  is less than the variance of  $E_B$  between different compositions, exploring compositional effects on  $E_B$  will be a fundamentally hopeless endeavor. Thus, it is expedient to develop novel measurement methods that are accurate, precise, and reproducible.

In order to address these challenges, I propose to develop a highly accurate and precise method using electroabsorption (EA) spectroscopy to measure  $E_B$  in 2D MHPs. This new measurement method will then be applied to a wide range of 2D MHP compounds using electroabsorption (EA) and dielectric spectroscopies in order to measure the exciton's binding energy, radius, mass, dipole moment, and polarizability and thereby establish exciton tunability in 2D MHPs.

### Specific Aims

1. Simulate the EA spectrum of a 2D Wannier exciton in order to better understand features in the EA spectrum of 2D MHPs and thereby develop a method for accurately measuring  $E_B$  in 2D MHPs.
2. Synthesize multiple 2D MHP compositions (elemental substitutions of A, B, and X into the generalized formula  $A_2BX_4$ ) and use EA spectroscopy to measure the band gap ( $E_G$ ) and exciton binding energy ( $E_B$ ) for each composition.
3. Use dielectric spectroscopy to measure the real part of the dielectric function  $\epsilon_r(\omega)$  for the barrier layer  $[A_2]^{2+}$ , well layer  $[BX_4]^{2-}$ , and the full 2D MHP material  $A_2BX_4$ .
4. Use mathematical models, based on the image charge and quantum-confinement effects, to convert the  $E_B$  and  $\epsilon_r$  measurements for 2D MHPs into theoretical values for 3D MHPs. Such models will be used to determine hypothetical  $E_B$  values for exfoliated 2D MHP sheets in a vacuum, and thereby contextualize our results within the universal scaling law for 2D systems, i.e.  $E_B \sim E_G/4$ .<sup>14</sup>

Two-dimensional metal-halide perovskites (2D MHPs) have become the focus of intense research efforts due to their unique charge-lattice interactions and impressive device performance in solar cells, LEDs, field-effect transistors, photodetectors, and polariton lasers.<sup>3, 15-18</sup> For theoretical and applied progress to continue forward, it is critical for the community to reach a consensus of basic photophysical properties such as  $E_B$  and  $E_G$ ; however, state-of-the art techniques to measure such values yield inconsistent results.<sup>12, 19</sup> For my PhD research I propose to use EA and dielectric spectroscopies along with theoretical models for excitons in layered systems, as represented in **Fig. 1**, to not only obtain unambiguous measurements of these values but also to develop models that can be used to predict  $E_B$  in 3D MHPs. In accomplishing the above aims, the exciton binding energy will turn from an unknown into a controllable degree of freedom for future MHP device engineering.

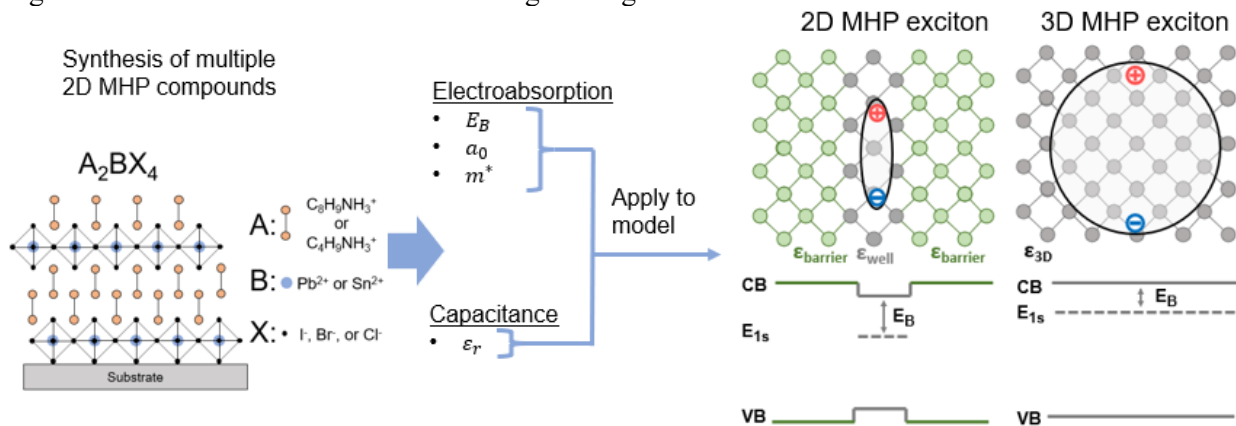


**Figure 1:** Pathway towards understand the effect of chemical substitutions on the 2D MHP exciton properties. First, six compounds:  $PEA_2PbI_4$ ,  $PEA_2SnI_4$ ,  $PEA_2PbBr_4$ ,  $PEA_2PbCl_4$ ,  $PEA_2SnBr_4$ ,  $PEA_2SnCl_4$  (where  $PEA = C_8H_9NH_3^+$ ) will be synthesized. The measured EA spectrum will yield the exciton's binding energy ( $E_B$ ), radius ( $a_0$ ), and mass ( $m^*$ ) while the measured capacitance will yield the material's dielectric constant ( $\epsilon_r$ ). These values will then be used to develop empirical models for  $E_B$  in 2D and 3D MHPs.

## Research Plan

### **Aim 1: Numerical simulation of the 2D MHP EA spectrum**

In pursuit of high confidence measurements of excitonic properties in 2D MHPs, I am motivated to turn to the technique that was most significant in advancing the fundamental understanding of III-IV quantum wells, namely electroabsorption spectroscopy (EA). EA measures the difference in a material's absorption spectrum,  $A$ , with and without an applied field:

$$\Delta A = A(F) - A(F = 0) \quad (1)$$

In the 1980's, the seminal work of Bastard, Mendez, and Miller,<sup>20-24</sup> based on the theory of Dow and Blossey,<sup>25, 26</sup> not only demonstrated the anisotropy of the inorganic quantum well electronic structure but also achieved a high level of agreement between theory and experiment<sup>27</sup> which lead to measurements of the exciton's Bohr radius  $a_0$ , reduced effective mass  $m^*$ , and  $E_B$ .

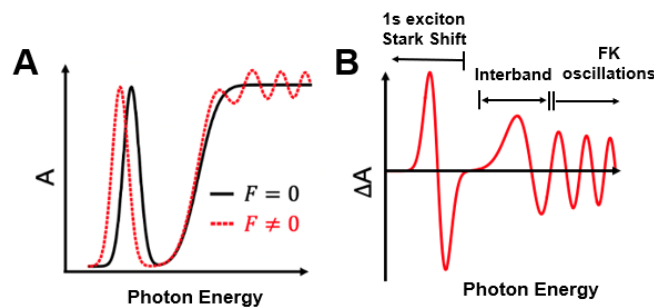


**Figure 2:** (A) Prototypical absorption (black) and field-shifted absorption of an excitonic semiconductor and the corresponding (B) EA signal  $A(F = 0) - A(F \neq 0)$ .

difficult to pinpoint  $E_G$  and leading to contradictory measurements of  $E_B$  (190 vs 361 meV for PEA<sub>2</sub>PbI<sub>4</sub><sup>28</sup>,<sup>29</sup> and 220 vs 364 meV for BA<sub>2</sub>PbI<sub>4</sub><sup>30, 31</sup>). It is important to note that the variance here originates from differing interpretations of nearly identical EA spectra. Indeed, the extremely close qualitative resemblance of the 2D MHP EA response in these four studies demonstrates the measurement is reliable and it is a lack of understanding, not measurement error, that has thus far impeded EA from producing reliable measurements of the exciton's properties. Therefore, the first aim of this study is the bridge the gap between the experimental EA features and our theoretical understanding of them by simulating the EA response of a 2D Wannier exciton in a uniform electric field in a regime that should be expected for 2D MHPs, i.e. a low-field and low-broadening regime. The same theory, in a high-field low-broadening regime was extremely successful in describing the EA response of III-V quantum wells.<sup>27</sup> However, this theory has thus far been overlooked in its application to 2D MHPs, perhaps in-part due to the fact a lengthy and complex numerical procedure is needed to solve the Schrödinger equation of a 2D Wannier exciton in a uniform field. In dimensionless units, this equation takes the following form:<sup>26</sup>

$$\left( -\nabla_{x,y}^2 - \frac{2}{r} + fx \right) \psi_n(x, y) = E_n \psi_n(x, y) \quad (2)$$

where  $\psi_n(x, y)$  is the wave function for the electron-hole relative motion,  $E_n$  is  $\hbar\omega - E_G$ ,  $f$  is a dimensionless field defined as the ratio between the applied electric field and the field required to create a potential drop of 1  $E_B$  across the exciton's radius (i.e. the ionization field), and is defined in terms of the material parameters, as follows:<sup>25</sup>

The standard absorption spectrum (Fig. 2(A)) and EA spectrum (Fig. 2(B)) for an excitonic semiconductor is divided into three regions: (1) below-gap where the exciton states redshift according to the Stark effect (2) near-gap where interband transitions are affected by the Franz-Keldysh (FK) effect and (3) above-gap where the same FK effect produces sinusoidal-like oscillations over a wide spectral range. The EA response of 2D MHPs closely resembles this behavior.<sup>28-31</sup> While the Stark shift of the 1s exciton is unambiguous in all reports of 2D MHP EA spectra, the near-gap and above-gap EA features are less straightforward making it

$$f = \frac{e^5}{128 \pi^3 \hbar \varepsilon_0} \frac{(m^*)^2}{(\varepsilon^*)^3} \quad (3)$$

where  $m^*$  is the exciton's reduced effective mass,  $\varepsilon^*$  is the effective dielectric constant,<sup>32</sup> and the physical constants  $e$ ,  $\hbar$ , and  $\varepsilon_0$  have their standard definitions. Assuming reasonable values for  $\varepsilon^*$  between 3 – 5 and a reduced effective mass  $m^*$  between  $0.050 - 0.221 m_0$ ,<sup>12, 33</sup> the ionization field for 2D MHPs is calculated to fall the range of  $10^2 - 10^4$  kV/cm, far greater than the maximum field strength that can be produced experimentally ( $\sim 30$  kV/cm). Therefore, the 2D MHP EA spectrum should be simulated in the low-field regime where ionization effects are negligible  $0.003 < f < 0.3$ . The final material parameter needed for the simulation is the homogenous broadening  $\Gamma$  which I have measured to be 11 meV by fitting a Lorentzian profile to the 1s exciton absorption peak.

To make **Eq. (2)** tractable, a transformation to parabolic coordinates is needed. This results in two quasi-Schrödinger equations with boundary conditions that have been determined by Dow and Blossey.<sup>25, 26</sup> My proficiency in using Matlab to solve differential equations will allow me to implement the numerical procedure that is described in detail in **Ref. (34)** and **Ref. (35)** in order to determine the electron-hole wavefunctions  $\psi_n(r)$  for a range of photon energies  $E$  and field strengths  $f$ .<sup>34, 35</sup> These wavefunctions relate to the semiconductor's absorption spectrum  $\alpha(E)$  through Elliot's formula for direct interband transitions:<sup>36, 37</sup>

$$\alpha(E, f) = B \sum_n |\psi_n(r = 0, f)|^2 \delta(E_n - \hbar\omega) \quad (4)$$

where  $B$  is a constant based on material parameters that can be set to unity for the purposes of simulating the EA line shape. The simulated EA spectrum is then calculated as:

$$\Delta\alpha = \alpha(E, f) * L(E) - \alpha(E) * L(E) \quad (5)$$

where  $L(E)$  is a Lorentzian function with a half-width-half-maximum (HWHM) of  $\Gamma$ . The resulting EA features of the 2D Wannier exciton and their positions, relative to  $E_G$  and  $E_{1s}$ , will allow for precise measurements of  $E_B$  and a deepened understanding of the 2D MHP EA response.

### **Aim 2: Measure the exciton properties for multiple $A_2BX_4$ compositions**

The results of the numerical simulation will be compared to the experimental EA spectra for a wide range of 2D MHP chemical compounds with general formula  $A_2BX_4$ . In the last decade, many photophysical studies on the prototypical 2D MHP material  $PEA_2PbI_4$  have led to a deepened understanding of the exciton physics and dynamic coupling to phonon modes within the  $[PbI_4]^{2-}$  layer.<sup>10, 38</sup> Simultaneously, many researchers have turned to the tin-based  $PEA_2SnI_4$  for the fabrication of field effect transistors (FET) and bromide and chloride varieties of  $PEA_2PbBr_4$  and  $PEA_2PbCl_4$  for the fabrication of UV photodetectors and LEDs.<sup>4, 17, 39, 40</sup> It is well established that the band gap increases moving from I to Br to Cl, and decreases moving from Pb to Sn. However, outside of the band gap, the effect of these chemical substitutions on the electronic structure and exciton properties remains largely unexplored, particularly from an experimental perspective.

First principle calculations starting with Hartree-Fock studies in the 1990s have been in agreement the occupant of the B-site metal center is most consequential in determining electronic structure.<sup>41-43</sup> The conduction band primarily consists of the B-site metal's highest-occupied p orbital, meanwhile the valence bands are largely comprised of the X-site halide's highest-occupied p orbital anti-bonded to the B-site metal's highest-occupied s orbital. On the other hand, the A-site organic molecule offers a valuable degree of tunability by modulating the dielectric environment and phonon modes, but has minimal effect on the band structure.<sup>10, 44, 45</sup> Therefore, to efficiently explore the space of electronic structure and exciton tunability in 2D MHPs, I will synthesize the following six compounds:  $PEA_2PbI_4$ ,  $PEA_2SnI_4$ ,  $PEA_2PbBr_4$ ,  $PEA_2PbCl_4$ ,  $PEA_2SnBr_4$ ,  $PEA_2SnCl_4$ . I choose phenethylammonium (PEA) as the A-site cation not only

because it is the most commonly studied, but also due to the fact 2D MHP crystals with PEA maintain a single structural phase between room and liquid-helium temperatures, which is rare for MHP systems.<sup>46</sup> This lack of phase transition will be ideal for EA measurements as it allows the absorption broadening to be reduced at low temperatures without introducing new spectral structures, e.g. additional exciton peaks from secondary crystalline phases. Wherein the EA spectra of these six compounds fails to produce a clear trend, supplementary compounds will be synthesized using a butylammonium (BA) cation in place of PEA. Since the electronic coupling between the molecule and semiconducting layers is negligible, comparison of BA-based compounds will serve as a secondary data point in elucidating the effect of B-site and X-site cations on the excitonic properties.

Each of the 2D MHP compositions will be synthesized using established spin-coating techniques to produce polycrystalline thin films.<sup>47,48</sup> In brief, the ammonia salt PEAX or BAX (where X = I, Cl, or Br) will be combined with a corresponding lead or tin salt with a matching halide ( $PbX_2$  or  $SnX_2$ ), dissolved in a 4:1 DMF:DMSO solvent, and pipetted onto a substrate for spin coating. It has been shown that this solvent ratio produces 2D MHPs with quantum well layers homogeneously stacked parallel to the substrate.<sup>49</sup> Achieving this orientation is critically important for probing the exciton's in-plane EA response, and therefore, my colleagues and I will collect grazing-incidence X-ray diffraction (GIXD) patterns in order to measure the distribution of crystallite orientations within the polycrystalline film.<sup>50</sup> The EA signal of the 2D MHP films will also be affected by the film's microstructure and average grain size. Disordered films will have broader absorption features, and therefore, smaller EA signals. Furthermore, small grains will reduce the probability of observing FK oscillations above the band gap, which are needed to measure needed for measuring  $m^*$ . These oscillations persist for a spectral range that is proportional to the mean free path of conduction band electrons, and therefore, will be absent in films with small grain sizes (< 100 nm for MHPs).<sup>51</sup> Thus, in order to target large grains and continuous-film microstructure for each composition, I will test three common spin-coating procedures (hotcast<sup>48</sup>, antisolvent,<sup>52</sup> and post-annealed<sup>53</sup>) and characterize the resulting film quality using optical microscopy, atomic force microscopy (AFM), and X-ray diffraction. The procedure that yields the highest quality film will then be used to spin-coat films for EA and dielectric spectroscopies.

The proposed methods for measuring the 2D MHP EA and dielectric spectra are highlighted in **Fig. 3**. An array of interdigitated fingers (**Fig. 3(A)**) will be used to produce high electric fields (5 – 30 kV/cm) parallel to the substrate while also allowing for the transmission of light. Postdoctoral scholar Hao-Chieh Hsieh will use photolithography to deposit gold electrodes onto quartz substrates in the University of Utah clean room. Perovskite films will then be spin-cast directly onto the substrate array for EA (**Fig. 3(B)**) and dielectric measurements (**Fig. 3(C)**). The EA procedure will be carried out in Dr. John Colton's laboratory in Brigham Young University and is as follows: first, samples are mounted into a cryostat, cooled to low temperature in order to reduce the homogenous broadening, and then the transmission of sample  $T$ , transmission of substrate  $T_0$ , and electro-transmission of sample  $\Delta T$  are collected as independent wavelength scans (set-up depicted in **Fig. 3(B)** for  $\Delta T$  mode). The absorption  $A(E)$  and EA spectra  $\Delta A(E)$  will then be calculated as:<sup>54</sup>

$$A = \log_{10}(T_0/T) \quad (6)$$

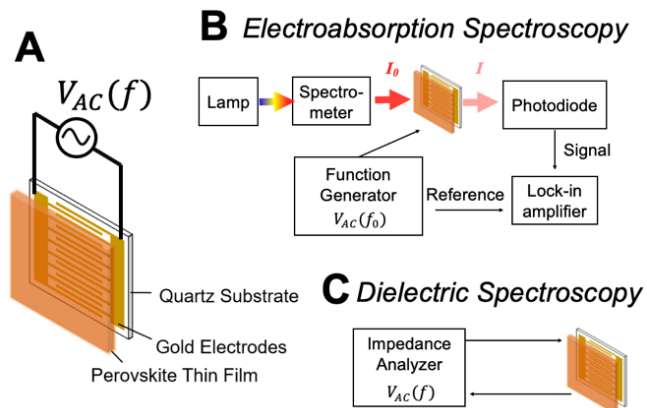


**Figure 3:** (A) Perovskite film cast on a substrate of interdigitated electrodes which can be used to measure the film's (B) EA response and (C) dielectric spectrum.

to reduce the homogenous broadening, and then the transmission of sample  $T$ , transmission of substrate  $T_0$ , and electro-transmission of sample  $\Delta T$  are collected as independent wavelength scans (set-up depicted in **Fig. 3(B)** for  $\Delta T$  mode). The absorption  $A(E)$  and EA spectra  $\Delta A(E)$  will then be calculated as:<sup>54</sup>

$$\Delta A = -\log_{10} \left( 1 + \frac{\Delta T}{T} \right) \quad (7)$$

The measured EA spectrum  $\Delta A(E)$  will be compared to the simulated EA spectra  $\Delta\alpha(E)$  for each 2D MHP composition. The relative alignment critical points in  $\Delta A(E)$ , relative to  $E_{1s}$  and  $E_G$  in  $\Delta\alpha(E)$ , will allow for determination of  $E_B = E_G - E_{1s}$ . Once  $E_B$  is measured with high-confidence, the field dependence of the Stark shift can be used to measure the exciton's transition dipole moment  $\mu$ , polarizability  $\alpha$ , and Bohr radius  $a_0$ .<sup>55</sup> If high-field Franz-Keldysh features are resolved, the exciton's reduced effective mass  $m^*$  can also be determined.<sup>56</sup> However, measurement of  $a_0$ ,  $\mu$ ,  $\alpha$ , and  $m^*$  requires knowledge of the electric field strength  $F$ , as experienced by the exciton, which depends on the real part of the dielectric function  $\varepsilon_r$  at the frequency of the modulating voltage signal,  $V_{AC}(f_0)$ . The dielectric properties of 2D MHPs have thus far not been reported in the literature, and therefore, it is necessary to develop a method to measure  $\varepsilon_r(f_0)$  for each 2D MHP thin film.

### **Aim 3: Measure dielectric values for multiple $A_2BX_4$ compositions**

Measuring the dielectric spectrum for each 2D MHP composition serves two critical roles in accomplishing the aims of this proposed research. First, knowledge of  $\varepsilon_r(f_0)$  will allow the exciton's properties  $a_0$ ,  $\mu$ ,  $\alpha$ , and  $m^*$  to be measured from the EA spectrum, as previously discussed. Second and equally importantly, the dielectric value near  $10^7$  Hz is an excellent measurement of the effective dielectric value ( $\varepsilon_r(10^7$  Hz)  $\approx \varepsilon^*$ )<sup>32, 57</sup> which is an important input parameter for the mathematical models of **Aim 4**. This is because  $E_B$  is primarily determined by  $\varepsilon^*$  and  $m^*$ , with the former carrying greater weight.<sup>14</sup>

Traditionally, the dielectric properties of MHPs are measured by pasting silver electrodes onto single crystals and recording the capacitance of the crystal in a parallel-plate geometry for a spectrum of AC frequencies. However, as we show in the following, the substrates with interdigitated electrode fingers can also be employed to directly measure dielectric properties of 2D MHP thin films (represented in **Fig. 3(C)**). This geometry will allow for facile dielectric measurements of the long list of thin film materials needed for this study, namely:  $PbX_2$ ,  $SnX_2$ ,  $PEA_2PbX_4$ ,  $PEA_2SnX_4$ ,  $C_3NH_3PbX_3$ ,  $C_3NH_3SnX_3$  where  $X = I$ , Br, or Cl (18 films total), without the need of growing single crystals. Thin films of metal-halide salts ( $PbX_2$ ,  $SnX_2$ ) and 3D MHPs ( $C_3NH_3PbX_3$ ,  $C_3NH_3SnX_3$ ) can be created with spin-coating procedures similar to the 2D MHP procedure,<sup>48, 58</sup> and the measured dielectric values will be used as input parameters for the mathematical models of **Aim 4**. As first shown by den Otter,<sup>59</sup> the capacitance ( $C$ ) of interdigitated electrodes in a uniform dielectric medium can be well-approximated by a summation of zeroth Bessel function of the first kind ( $J_0$ ). My collaborator Emma McClure modified den Otter's equations to fit a thin film geometry in order to account for the independent dielectric loads of the quartz substrate ( $\varepsilon_{r,q} = 3.7$ ),<sup>60</sup> the thin film ( $\varepsilon_{r,f}$ ), and air ( $\varepsilon_{r,a} = 1$ ), as follows:

$$C = \frac{pq\pi}{8V_0a} \sum_{n=1}^{\infty} \frac{J_0\left(\frac{(2n-1)\pi s}{2a}\right)}{2n-1} [\varepsilon_{r,q}(1 - e^{(2-4n)\pi t_q/a}) + \varepsilon_{r,f}(1 - e^{(2-4n)\pi t_f/a}) + \varepsilon_{r,a}(e^{(2-4n)\pi t_q/a} + e^{(2-4n)\pi t_f/a})] \quad (8)$$

where  $p$ ,  $q$ ,  $s$ , and  $a$  denote various dimensions of the interdigitated electrodes and  $t_q$  and  $t_f$  denote the thickness of the quartz substrate and thin film, respectively. Optical profilometry and AFM in the University of Utah Nanofab will be used to measure  $t_f$ . The 2D MHP thin films will be cast onto interdigitated electrodes and electrically connected to the input of an impedance analyzer. The capacitance across a wide frequency range ( $10^0 - 10^7$  Hz) will be recorded, and with the use **Eq. (8)**, these capacitance values will be used to obtain  $\varepsilon_{r,f}$ .

### **Aim 4: Mathematical model for $E_B$ in MHPs**

While the hydrogenic formalism of **Eq (2)** represents the state-of-the-art theoretical description of a 2D MHP exciton in an electric field, more sophisticated theoretical models exist for describing 2D MHP excitons in the absence of external electric fields.<sup>12, 61, 62</sup> Excitons in 2D MHPs deviate from the hydrogen model primarily due to: (1) their non-zero spatial extent in the  $\hat{z}$  direction which results in a level of quantum confinement that is less than the 2D case and (2) their anisotropic dielectric environment which results in an  $E_B$ -enhancing image charge effect. In a simple model, the hydrogenic expression for  $E_B$  can be modified to account for these two effects, as follows:

$$E_B = \left(\frac{\varepsilon_w}{\varepsilon_b}\right)^\gamma \left(\frac{2}{\alpha - 1}\right)^2 \left(\frac{1}{\varepsilon^*}\right)^2 \left(\frac{m^*}{m_0}\right) R_H \quad (9)$$

where  $\varepsilon_w$  is the dielectric of the well layer ( $[BX_4]^{2+}$ ),  $\varepsilon_b$  is the dielectric of the barrier layer ( $[PEA_2]^{2+}$ ),  $\gamma$  is a real number that has yet to be empirically determined,  $\alpha$  is the fractional dimensionality,  $m_0$  is the electron mass, and  $R_H$  is the Rydberg energy of hydrogen. The first factor  $(\varepsilon_w/\varepsilon_b)^\gamma$  in **Eq. (9)** accounts for the image-charge effect on  $E_B$ <sup>61, 63</sup> while the second factor  $(2/(\alpha - 1))^2$  accounts for quantum confinement in a fractional-dimensional ( $\alpha$ -D) system.<sup>64</sup> In a purely 2D system, the dimensionality  $\alpha = 2$  results in a factor of 4 enhancement and  $E_{B,2D} = 4E_{B,3D}$ . In 2D MHPs, however, the nonzero thickness of the well layer leads to  $\alpha = 2.3$ , as measured by Tanaka et al.<sup>65</sup> The values of  $E_B$  and  $m^*$  will be known from the EA spectrum,  $\varepsilon_w$  will be approximated by the dielectric constants of the  $PbX_2$  and  $SnX_2$  thin films,  $\varepsilon_r(10^7 \text{ Hz})$  of the 2D MHP film will be taken as  $\varepsilon^*$ , and the value  $\varepsilon_b = 3.32$  is known from dielectric measurements of PEA in the literature.<sup>33</sup> Therefore, all variables in **Eq. (9)** will be known, except for  $\gamma$ , for six 2D MHP compositions. Thus,  $\gamma$  will be empirically determined and the validity of **Eq. (9)** will be established by the standard deviation of  $\gamma$  across the six 2D MHP compositions.

Provided that **Eq. (9)** is found to be a good approximation, the  $E_B$  values for 2D MHPs can be converted to theoretical  $E_B$  values for 3D MHPs, as follows:

$$E_{B,2D} = \left(\frac{\varepsilon_w}{\varepsilon_b}\right)^\gamma \left(\frac{2}{\alpha - 1}\right)^2 \left(\frac{\varepsilon_{3D}^*}{\varepsilon_{2D}^*}\right)^2 E_{B,3D} \quad (10)$$

where  $\varepsilon_{3D}^*$  will be known from dielectric measurements of  $CH_3NH_3PbX_3$  and  $CH_3NH_3SnX_3$ . This expression assumes  $m_{2D}^* = m_{3D}^*$  which has been found to be a good approximation by numerous computation and experimental studies<sup>12, 42, 66-68</sup> due to the fact the 2D and 3D MHP electronic structures originate from the same metal-halide orbitals. Thus, the tunability of  $E_B$  for the class of 3D MHP materials can be reasonably estimated from  $E_B$  measurements on 2D MHPs. This is important because, while 3D MHPs are extremely impactful optoelectronic materials,<sup>69</sup> the variance in experimental and computational estimates for  $E_B$  (5 – 50 meV)<sup>70-72</sup> far exceeds the variance between different chemical compositions.

In addition to the calculations detailed above, I will also reach out to establish a collaboration with Dr. Jacky Even and Dr. Claudine Katan who are the world's expert in modeling dielectric and quantum confinement in 2D MHP using state-of-the-art theoretical models. The  $E_B$ ,  $a_0$ , and  $m^*$  from the EA spectrum can be used to improve Dr. Even's and Dr. Katan's models of the dielectric anisotropy in 2D MHPs. These improved models can then be used to predict the magnitude of  $E_B$  enhancement expected for exfoliated single layers on a variety of substrates and no substrate ( $\varepsilon_b = 1$ ).

#### Proposed Timeline:

Aim 1	Develop simulation		
Aim 2	Optimize fabrication	Collect EA	
Aim 3	Spin-coat 2D and 3D MHPs	Measure $\varepsilon_r$	
Aim 4		Identify state-of-the-art models	Calculate dielectric effects on $E_B$
Collaboration			
	Year 1		Year 2

### Challenges and Alternative Approaches

#### *Experimental artifacts in EA spectroscopy*

In general, modulation spectroscopies such as EA are trustworthy since the normalized difference signal  $\Delta T/T$  is free of the instrument response function. However, modulation of the transmission can sometimes result from phenomena other than field-induced changes in the absorption. These phenomena include: (1) field-induced changes in the refractive index ( $\Delta n$ ) and (2) thermal-induced changes in the absorption from Joule heating. I plan to calculate the magnitude of these two effects in order to estimate their contribution to the EA response of 2D MHPs. A Taylor expansion of the EA signal in terms of small changes in the refractive index  $\Delta n$  and absorption coefficient  $\Delta\alpha$  results in the following expression:<sup>73</sup>

$$\Delta A = C_1 \Delta n + C_2 \Delta\alpha - \Delta\alpha t_f \quad (11)$$

where  $C_1$  and  $C_2$  are optical constants that depend on the real  $n$  and imaginary  $\kappa$  components of the refractive index (expressions given in Ref. (73)) and  $t_f$  is the film thickness. Thus, the influence of field-induced changes in the 2D MHP refractive index on the EA signal can be estimated provided that  $n$  and  $\kappa$  are known across the spectral range of interest. I plan use a Kramer's Kroning analysis of the transmission data to calculate the  $n$  and  $\kappa$ , according to the method in Ref. (74).<sup>74</sup> The values of  $C_1$  and  $C_2$  will then be computed to determine their contribution to the EA signal. If refractive index effects are found to be large, I will consider using a simulated  $\Delta n$  (by a Kramer's Kroning transformation of the simulated  $\Delta\alpha$ ) to subtract  $C_1 \Delta n$  from the EA signal.

The contribution of thermal effects to the EA signal can be estimated by:<sup>73</sup>

$$\Delta A_{thermal} = \frac{dA}{dE} \frac{dE_G}{dT} \Delta T \quad (12)$$

where  $T$  now denotes temperature, not transmission.  $\Delta T$  is the RMS modulation of the temperature at the lock-in's reference frequency  $f_0$  and  $dE_G/dT$  is the rate of the band gap's blueshift with temperature ( $\sim 0.2$  meV/K for 2D MHPs).<sup>75</sup> The value of  $\Delta T$  can calculated from a power-balance equation: Power in – Power out =  $CdT/dt$  where  $C$  is the heat capacity of the substrate. The ‘power in’ terms include contributions from light absorption and Joule heating, the latter of which will be larger for the tin-based perovskites due to their higher electrical conductivity, while the ‘power out’ will represent the thermal contact with the cold finger. I will set up this power balance equation, solve for  $T(t)$ , and use the RMS value at the modulation frequency ( $\Delta T$ ) to calculate  $\Delta A_{thermal}$  in Eq. (12). If thermal effects are found to be large, I will consider using chemical additives to increase the resistivity of the perovskite film.<sup>76</sup>

### **High measurement uncertainty**

The proposed method for measuring  $m^*$  requires that FK features in the EA spectrum show a clear and consistent rate of field-broadening,<sup>56</sup> which may not be the case for all 2D MHP compositions. If the clarity and reproducibility of field-broadening within the FK features is poor, then I will establish a collaboration with an expert in using first principle approaches, such as density functional theory (DFT), to model MHP systems. DFT has proven effective at accurately determining  $m^*$  in MHP systems from the band curvature at  $k = 0$ .<sup>77</sup>

Another measurement that may prove to have high uncertainty is  $\epsilon_w$ , i.e. the dielectric value of the well layer ( $[BX_4]^{2-}$ ). Using the  $\epsilon_{r,f}(10^7 \text{ Hz})$  value of a  $BX_2$  thin film to estimate  $\epsilon_w$  may be an unfriendly approximation due to differing LO phonon contributions to  $\epsilon_r$  between  $BX_4$  2D sheets and  $BX_2$  3D lattices. Fortunately, the validity of this measurement can be easily assessed using the following expression for the quantum well's dielectric value:<sup>61</sup>

$$\epsilon_r = \frac{\epsilon_w L_w + \epsilon_b L_b}{L_w + L_b} \quad (13)$$

where  $L_w$  and  $L_b$  are the length of the well and barrier layers, respectively. If  $\epsilon_r$  from Eq. (13) differs from the measured dielectric value for multiple of the six 2D MHP compositions, then it will be known that using BX<sub>2</sub> films to estimate  $\epsilon_w$  is a poor approximation. In such a case,  $\epsilon_w$  will also be determined using DFT modeling. While the magnitude of the polarization contributions from valance electrons and phonons to a material's dielectric constant is sometimes difficult to accurately determine with first principle approaches, DFT calculations are comparatively more effective at capturing relative differences between materials, provided the same methodology is used. Therefore,  $\epsilon_b$  for the barrier layer [PEA<sub>2</sub>]<sup>2+</sup> will be calculated along with  $\epsilon_w$  to arrive at an accurate ratio ( $\epsilon_w/\epsilon_b$ ) that is needed for Eq. (9) and Eq. (10).

### Preliminary Results:

My colleagues and I have made significant progress carrying out the proposed research for the commonly-researched PEA<sub>2</sub>PbI<sub>4</sub> material. In Fig. 3, the measured absorption and EA spectra of PEA<sub>2</sub>PbI<sub>4</sub> (Fig. 3(A)) is shown in comparison the theoretical absorption and EA spectrum (Fig. 3(B)) simulated using the theory of Dow and Lederman.<sup>34</sup> The measured and simulated spectra have a high level of qualitative agreement. It was found that the zero-crossing of the exciton and interband (IB) features, labeled at 'b' and 'e' respectively in Fig. (3A), are the correct markers of  $E_{1s}$  and  $E_G$ . Thus,  $E_B = E_G - E_{1s}$  ( $\Delta be$ ) was measured to be  $223 \pm 3$  meV. Turning to reported EA spectra in the literature, we find that the positions of 'b' and 'e' are remarkable consistent across various studies which employ different procedures for sample fabrication and for EA measurements. As summarized in Table 1, our  $\Delta be$  measurement method yields  $E_B$  values with  $1\sigma$  variance of  $\sim 3$  meV for these EA spectra of PEA<sub>2</sub>PbI<sub>4</sub> and BA<sub>2</sub>PbI<sub>4</sub> in the literature, thus demonstrating that EA is a remarkable effective and reproducible technique when applied to 2D MHPs.

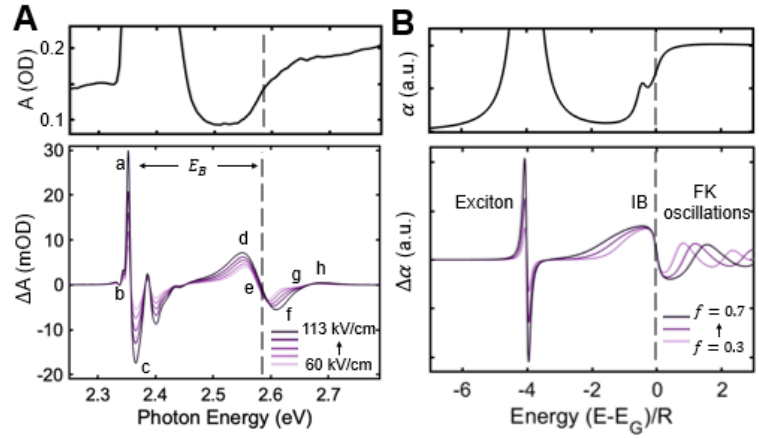


**Figure 4:** (A) Absorption (top) and EA (bottom) spectra for PEA<sub>2</sub>PbI<sub>4</sub> at 14 K in comparison with (B) the simulated absorption (top) and EA (bottom) spectra for a 2D Wannier exciton in the low-field, low-broadening regime.

**Table 1:** Comparison of  $E_B$  values from the literature, as measured by the  $\Delta be$  method

Material	Temp. (K)	$E_{1s}$ (b) (meV)	$E_G$ (e) (meV)	$E_B$ ( $\Delta be$ ) (eV)	Reported $E_B$ (eV)	Ref
PEA <sub>2</sub> PbI <sub>4</sub>	15	2.357	2.579	$223 \pm 3$	223	Hansen et al <sup>54</sup>
PEA <sub>2</sub> PbI <sub>4</sub>	50	2.38	2.60	$220 \pm 5$	190	<sup>28</sup>
BA <sub>2</sub> PbI <sub>4</sub>	45	2.551	2.802	$251 \pm 2$	251	Hansen et al <sup>54</sup>
BA <sub>2</sub> PbI <sub>4</sub>	50	2.550	2.800	$250 \pm 5$	220	<sup>30</sup>
BA <sub>2</sub> PbI <sub>4</sub>	45	2.561	2.814	$253 \pm 5$	340	<sup>31</sup>

The dielectric value of PEA<sub>2</sub>PbI<sub>4</sub> was measured using both parallel plate and interdigitated electrode geometries. The two methods were in agreement and we found  $\epsilon_r(f_0)$  to be 4.5. Knowledge of  $E_B$  and  $\epsilon_r(f_0)$  allowed for determination of the exciton's Bohr radius ( $a_0 = 2.2 \pm 0.55$  nm), transition dipole moment ( $\mu = 13 \pm 4$  D), and polarizability ( $\alpha = 80000 \pm 10300 \text{ \AA}^3$ ) according to the field dependence of the exciton's Stark shift as well as the reduced effective mass ( $m^* = 0.09 \pm 0.024 m_0$ ) according to the field

dependence of IB feature. These results have been summarized in a manuscript which is under review at *PRX Energy* and currently available for viewing on arXiv.org.<sup>54</sup>

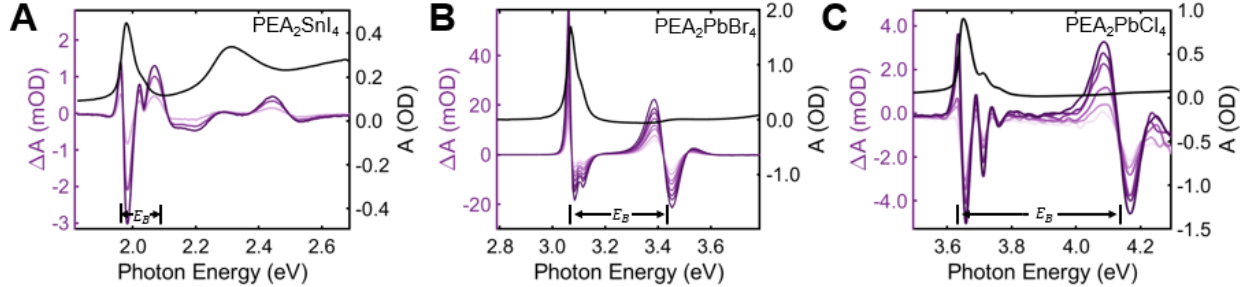


**Figure 5:** EA (purple) and absorption (black) spectra for (A)  $\text{PEA}_2\text{SnI}_4$  showing  $E_B = 100$  meV, (B)  $\text{PEA}_2\text{PbBr}_4$  showing  $E_B = 348$  meV, and (C)  $\text{PEA}_2\text{PbCl}_4$  showing  $E_B = 487$  meV.

While the dielectric constants of other 2D MHP compositions have yet to be measured, I have measured low-temperature EA spectra for three other compositions:  $\text{PEA}_2\text{SnI}_4$  (**Fig. 5(A)**),  $\text{PEA}_2\text{PbBr}_4$  (**Fig. 5(B)**), and  $\text{PEA}_2\text{PbCl}_4$  (**Fig. 5(C)**) resulting in accurate and precise determination of  $E_G$  and  $E_B$ . In **Fig. 6**, I plot relationship between  $E_G$  and  $E_B$  for 2D MHPs in comparison to the universal scaling law for 2D materials, that is,  $E_B \sim E_G/4$ .<sup>14</sup> It is clear the  $E_B$  values in 2D MHPs are highly tunable, from 100 meV for  $\text{PEA}_2\text{SnI}_4$  to 487 meV for  $\text{PEA}_2\text{PbCl}_4$  and that 2D MHPs in bulk form give access to a range of parameter space (low  $E_G$ , high  $E_B$ ) that is unique for semiconductors. This is undoubtably due to the factor of  $\sim 3$  enhancement to  $E_B$  that occurs as a result of the image charge effect. These data serve as unambiguous correction to previous studies that report  $E_B$  decreases moving from I to Br to Cl and stays relatively constant moving from Pb to Sn.<sup>19, 41, 63</sup>

Upon obtaining dielectric measurements and EA measurements for a wider range of 2D MHP compositions, my colleagues and I will be able to empirically determine  $\gamma$ , i.e. the power relation between the dielectric mismatch ( $\epsilon_w/\epsilon_b$ ) and the magnitude of the image charge effect on  $E_B$ . Using  $\epsilon_b = 1$ , it will be possible to predict  $E_B$  for exfoliated sheets of 2D MHPs in a vacuum and compare the resulting  $E_B$  values to the universal trendline  $E_B \sim E_G/4$ .

### Conclusion/Outlook:

Two- and three-dimensional MHPs are the star optoelectronic materials of this decade, but the development of tunable optoelectronic properties in MHPs has thus far been limited. Unlike III-V quantum wells, compositional changes to the 2D MHP structure is the primary pathway available for tuning the exciton's properties in this class of quantum wells. However, the variance between reported  $E_B$  values for a given  $\text{A}_2\text{BX}_4$  composition (in the 2D case) or a given  $\text{ABX}_3$  composition (in the 3D case) is the same order of magnitude as the expected variance between different chemical compositions. Therefore, establishing exciton tunability in MHP systems is a fundamentally hopeless endeavor until a precise, accurate, and reproducible method for measuring  $E_B$  is developed.

The four aims of this proposed work directly address this challenge and establish exciton tunability in MHPs. I will simulate the 2D MHP EA spectrum in **Aim 1** to gain a deeper understanding of the features within the experimental EA spectrum of 2D MHPs. The preliminary results show that this leads to consistent and reliable measurements of  $E_B$ . In **Aim 2**, I will exploit the sensitivity of EA spectroscopy and the large spectroscopic separation of exciton and continuum states in 2D MHPs to obtain high-confidence

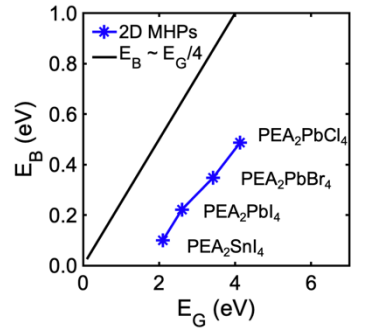


**Figure 6:** 2D MHPs in comparison to the universal scaling law for 2D materials  $E_B \sim E_G/4$ .

measurements of  $E_B$  for a wide range of  $A_2BX_4$  compositions ( $A = \text{PEA}$ ,  $B = \text{Pb}$  or  $\text{Sn}$ ,  $X = \text{I}$ ,  $\text{Br}$ , or  $\text{Cl}$ ). These measurements will be complemented with dielectric spectroscopy in **Aim 3** and the measured values will be used as input parameters for empirical (and potentially theoretical) models, as described in **Aim 4**, to establish exciton tunability in this important class of materials. These are important steps towards the development of next-generation photovoltaics, LEDs, and other optoelectronic devices.

## References

1. Nakamura, S.; Senoh, M.; Iwasa, N.; Nagahama, S.-i., High-brightness InGaN blue, green and yellow light-emitting diodes with quantum well structures. *Jpn. J. Appl. Phys.* **1995**, *34* (7A), L797.
2. Nakamura, S.; Senoh, M.; Iwasa, N.; Nagahama, S.-i.; Yamada, T.; Mukai, T., Superbright green InGaN single-quantum-well-structure light-emitting diodes. *Jpn. J. Appl. Phys.* **1995**, *34* (10B), L1332.
3. Yuan, M.; Quan, L. N.; Comin, R.; Walters, G.; Sabatini, R.; Voznyy, O.; Hoogland, S.; Zhao, Y.; Beauregard, E. M.; Kanjanaboos, P.; Lu, Z.; Kim, D. H.; Sargent, E. H., Perovskite energy funnels for efficient light-emitting diodes. *Nat. Nanotechnol.* **2016**, *11* (10), 872-877.
4. Byun, J.; Cho, H.; Wolf, C.; Jang, M.; Sadhanala, A.; Friend, R. H.; Yang, H.; Lee, T. W., Efficient visible quasi-2D perovskite light-emitting diodes. *Adv. Mater.* **2016**, *28* (34), 7515-7520.
5. Grancini, G.; Roldán-Carmona, C.; Zimmermann, I.; Mosconi, E.; Lee, X.; Martineau, D.; Narbey, S.; Oswald, F.; De Angelis, F.; Graetzel, M., One-Year stable perovskite solar cells by 2D/3D interface engineering. *Nat. Commun.* **2017**, *8* (1), 1-8.
6. Mao, L.; Stoumpos, C. C.; Kanatzidis, M. G., Two-dimensional hybrid halide perovskites: principles and promises. *J. Am. Chem. Soc.* **2018**, *141* (3), 1171-1190.
7. Amano, H.; Sawaki, N.; Akasaki, I.; Toyoda, Y., Metalorganic vapor phase epitaxial growth of a high quality GaN film using an AlN buffer layer. *Appl. Phys. Lett.* **1986**, *48* (5), 353-355.
8. Amano, H.; Kito, M.; Hiramatsu, K.; Akasaki, I., P-type conduction in Mg-doped GaN treated with low-energy electron beam irradiation (LEEBI). *Jpn. J. Appl. Phys.* **1989**, *28* (12A), L2112.
9. Akasaki, I.; Amano, H.; Koide, Y.; Hiramatsu, K.; Sawaki, N., Effects of ain buffer layer on crystallographic structure and on electrical and optical properties of GaN and  $\text{Ga}_{1-x}\text{Al}_x\text{N}$  ( $0 < x \leq 0.4$ ) films grown on sapphire substrate by MOVPE. *J. Cryst. Growth* **1989**, *98* (1-2), 209-219.
10. Thouin, F.; Valverde-Chávez, D. A.; Quarti, C.; Cortecchia, D.; Bargigia, I.; Beljonne, D.; Petrozza, A.; Silva, C.; Srimath Kandada, A. R., Phonon coherences reveal the polaronic character of excitons in two-dimensional lead halide perovskites. *Nat. Mater.* **2019**, *18* (4), 349-356.
11. Miyata, A.; Mitioglu, A.; Plochocka, P.; Portugall, O.; Wang, J. T.-W.; Stranks, S. D.; Snaith, H. J.; Nicholas, R. J., Direct measurement of the exciton binding energy and effective masses for charge carriers in organic-inorganic tri-halide perovskites. *Nat. Phys.* **2015**, *11* (7), 582-587.
12. Blancon, J. C.; Stier, A. V.; Tsai, H.; Nie, W.; Stoumpos, C. C.; Traoré, B.; Pedesseau, L.; Kepenekian, M.; Katsutani, F.; Noe, G. T.; Kono, J.; Tretiak, S.; Crooker, S. A.; Katan, C.; Kanatzidis, M. G.; Crochet, J. J.; Even, J.; Mohite, A. D., Scaling law for excitons in 2D perovskite quantum wells. *Nat. Commun.* **2018**, *9* (1), 2254.
13. Yaffe, O.; Chernikov, A.; Norman, Z. M.; Zhong, Y.; Velauthapillai, A.; van der Zande, A.; Owen, J. S.; Heinz, T. F., Excitons in ultrathin organic-inorganic perovskite crystals. *Phys. Rev. B* **2015**, *92* (4), 045414.
14. Jiang, Z.; Liu, Z.; Li, Y.; Duan, W., Scaling universality between band gap and exciton binding energy of two-dimensional semiconductors. *Phys. Rev. Lett.* **2017**, *118* (26), 266401.
15. Zhang, T.; Dar, M. I.; Li, G.; Xu, F.; Guo, N.; Grätzel, M.; Zhao, Y., Bication lead iodide 2D perovskite component to stabilize inorganic  $\alpha\text{-CsPbI}_3$  perovskite phase for high-efficiency solar cells. *Sci. Adv.* **2017**, *3* (9), e1700841.
16. Fieramosca, A.; Polimeno, L.; Ardizzone, V.; De Marco, L.; Pugliese, M.; Maiorano, V.; De Giorgi, M.; Dominici, L.; Gigli, G.; Gerace, D., Two-dimensional hybrid perovskites sustaining strong polariton interactions at room temperature. *Sci. Adv.* **2019**, *5* (5), eaav9967.

17. Tan, Z.; Wu, Y.; Hong, H.; Yin, J.; Zhang, J.; Lin, L.; Wang, M.; Sun, X.; Sun, L.; Huang, Y., Two-dimensional ( $C_4H_9NH_3$ ) $_2PbBr_4$  perovskite crystals for high-performance photodetector. *J. Am. Chem. Soc.* **2016**, *138* (51), 16612-16615.
18. Chen, Y.; Sun, Y.; Peng, J.; Tang, J.; Zheng, K.; Liang, Z., 2D Ruddlesden-Popper perovskites for optoelectronics. *Adv. Mater.* **2018**, *30* (2), 1703487.
19. Dyksik, M.; Duim, H.; Zhu, X.; Yang, Z.; Gen, M.; Kohama, Y.; Adjokatse, S.; Maude, D. K.; Loi, M. A.; Egger, D. A., Broad tunability of carrier effective masses in two-dimensional halide perovskites. *ACS Energy Lett.* **2020**, *5* (11), 3609-3616.
20. Miller, D. A. B.; Chemla, D. S.; Damen, T. C.; Gossard, A. C.; Wiegmann, W.; Wood, T. H.; Burrus, C. A., Band-Edge Electroabsorption in Quantum Well Structures: The Quantum-Confining Stark Effect. *Phys. Rev. Lett.* **1984**, *53* (22), 2173-2176.
21. Miller, D. A. B.; Chemla, D. S.; Damen, T. C.; Gossard, A. C.; Wiegmann, W.; Wood, T. H.; Burrus, C. A., Electric field dependence of optical absorption near the band gap of quantum-well structures. *Phys. Rev. B.* **1985**, *32* (2), 1043-1060.
22. Bastard, G.; Mendez, E.; Chang, L.; Esaki, L., Exciton binding energy in quantum wells. *Phys. Rev. B.* **1982**, *26* (4), 1974.
23. Bastard, G.; Mendez, E.; Chang, L.; Esaki, L., Variational calculations on a quantum well in an electric field. *Phys. Rev. B.* **1983**, *28* (6), 3241.
24. Mendez, E.; Agullo-Rueda, F.; Hong, J., Stark localization in GaAs-GaAlAs superlattices under an electric field. *Phys. Rev. Lett.* **1988**, *60* (23), 2426.
25. Dow, J. D.; Redfield, D., Electroabsorption in Semiconductors: The Excitonic Absorption Edge. *Phys. Rev. B.* **1970**, *1* (8), 3358-3371.
26. Blossey, D. F., Wannier exciton in an electric field. II. Electroabsorption in direct-band-gap solids. *Phys. Rev. B.* **1971**, *3* (4), 1382.
27. Kneissl, M.; Linder, N.; Kiesel, P.; Quassowski, S.; Schmidt, K.; Döhler, G. H.; Grothe, H.; Smith, J. S., Two-dimensional Franz-Keldysh effect in MQW structures with lateral electric fields. *Superlattices Microstruct.* **1994**, *16* (2), 109.
28. Zhai, Y.; Baniya, S.; Zhang, C.; Li, J.; Haney, P.; Sheng, C.-X.; Ehrenfreund, E.; Vardeny, Z. V., Giant Rashba splitting in 2D organic-inorganic halide perovskites measured by transient spectroscopies. *Sci. Adv.* **2017**, *3* (7), e1700704.
29. Tanaka, K.; Kondo, T., Bandgap and exciton binding energies in lead-iodide-based natural quantum-well crystals. *Sci. Technol. Adv. Mater.* **2003**, *4* (6), 599-604.
30. Amerling, E.; Baniya, S.; Lafalce, E.; Zhang, C.; Vardeny, Z. V.; Whittaker-Brooks, L., Electroabsorption Spectroscopy Studies of  $(C_4H_9NH_3)_2PbI_4$  Organic-Inorganic Hybrid Perovskite Multiple Quantum Wells. *J. Phys. Chem. Lett.* **2017**, *8* (18), 4557-4564.
31. Kattoor, V.; Awasthi, K.; Jokar, E.; Diau, E. W.-G.; Ohta, N., Integral Method Analysis of Electroabsorption Spectra and Electrophotoluminescence Study of  $(C_4H_9NH_3)_2PbI_4$  Organic-Inorganic Quantum Well. *J. Phys. Chem. C* **2018**, *122* (46), 26623-26634.
32. Umari, P.; Mosconi, E.; De Angelis, F., Infrared Dielectric Screening Determines the Low Exciton Binding Energy of Metal-Halide Perovskites. *J. Phys. Chem. Lett.* **2018**, *9* (3), 620-627.
33. Hong, X.; Ishihara, T.; Nurmikko, A., Dielectric confinement effect on excitons in PbI<sub>4</sub>-based layered semiconductors. *Phys. Rev. B.* **1992**, *45* (12), 6961.
34. Lederman, F. L.; Dow, J. D., Theory of electroabsorption by anisotropic and layered semiconductors. I. Two-dimensional excitons in a uniform electric field. *Phys. Rev. B.* **1976**, *13* (4), 1633-1642.
35. Zhang, X. A Planar Violet Electroabsorption Modulator and Modeling of Electric Effects on Zinc Oxide Excitons. North Carolina State University, 2006.
36. Elliott, R., Intensity of optical absorption by excitons. *Phys. Rev.* **1957**, *108* (6), 1384.
37. Galbraith, I., Excitonic electroabsorption and electrorefraction in semiconductors. *Phys. Rev. B.* **1993**, *48* (8), 5105.

38. Neutzner, S.; Thouin, F.; Cortecchia, D.; Petrozza, A.; Silva, C.; Srimath Kandada, A. R., Exciton-polaron spectral structures in two-dimensional hybrid lead-halide perovskites. *Phys. Rev. Mater.* **2018**, *2* (6), 064605.
39. Chen, C.; Zhang, X.; Wu, G.; Li, H.; Chen, H., Visible-Light Ultrasensitive Solution-Prepared Layered Organic-Inorganic Hybrid Perovskite Field-Effect Transistor. *Advanced Optical Materials* **2017**, *5* (2), 1600539.
40. Matsushima, T.; Hwang, S.; Sandanayaka, A. S.; Qin, C.; Terakawa, S.; Fujihara, T.; Yahiro, M.; Adachi, C., Solution-processed organic-inorganic perovskite field-effect transistors with high hole mobilities. *Adv. Mater.* **2016**, *28* (46), 10275-10281.
41. Papavassiliou, G. C.; Koutselas, I. B.; Terzis, A.; Whangbo, M. H., Structural and electronic properties of the natural quantum-well system (C<sub>6</sub>H<sub>5</sub>CH<sub>2</sub>CH<sub>2</sub>NH<sub>3</sub>)<sub>2</sub>SnI<sub>4</sub>. *Solid State Commun.* **1994**, *91* (9), 695-698.
42. Zibouche, N.; Islam, M. S., Structure-Electronic Property Relationships of 2D Ruddlesden-Popper Tin- and Lead-based Iodide Perovskites. *ACS Appl. Mater. Interfaces* **2020**, *12* (13), 15328-15337.
43. Pazoki, M.; Jacobsson, T. J.; Hagfeldt, A.; Boschloo, G.; Edvinsson, T., Effect of metal cation replacement on the electronic structure of metalorganic halide perovskites: Replacement of lead with alkaline-earth metals. *Phys. Rev. B* **2016**, *93* (14), 144105.
44. Phuyal, D.; Safdari, M.; Pazoki, M.; Liu, P.; Philippe, B.; Kvashnina, K. O.; Karis, O.; Butorin, S. M.; Rensmo, H.; Edvinsson, T., Electronic structure of two-dimensional lead (ii) iodide perovskites: an experimental and theoretical study. *Chem. Mater.* **2018**, *30* (15), 4959-4967.
45. Li, J.; Rinke, P., Atomic structure of metal-halide perovskites from first principles: The chicken-and-egg paradox of the organic-inorganic interaction. *Phys. Rev. B* **2016**, *94* (4), 045201.
46. Miyata, K.; Atallah, T. L.; Zhu, X.-Y., Lead halide perovskites: Crystal-liquid duality, phonon glass electron crystals, and large polaron formation. *Sci. Adv.* **2017**, *3* (10), e1701469.
47. Cao, D. H.; Stoumpos, C. C.; Farha, O. K.; Hupp, J. T.; Kanatzidis, M. G., 2D Homologous Perovskites as Light-Absorbing Materials for Solar Cell Applications. *J. Am. Chem. Soc.* **2015**, *137* (24), 7843-7850.
48. Nie, W.; Tsai, H.; Asadpour, R.; Blancon, J.-C.; Neukirch, A. J.; Gupta, G.; Crochet, J. J.; Chhowalla, M.; Tretiak, S.; Alam, M. A.; Wang, H.-L.; Mohite, A. D., High-efficiency solution-processed perovskite solar cells with millimeter-scale grains. *Science* **2015**, *347* (6221), 522.
49. Cao, D. H.; Stoumpos, C. C.; Yokoyama, T.; Logsdon, J. L.; Song, T.-B.; Farha, O. K.; Wasielewski, M. R.; Hupp, J. T.; Kanatzidis, M. G., Thin Films and Solar Cells Based on Semiconducting Two-Dimensional Ruddlesden-Popper (CH<sub>3</sub>(CH<sub>2</sub>)<sub>3</sub>NH<sub>3</sub>)<sub>2</sub>(CH<sub>3</sub>NH<sub>3</sub>)<sub>n-1</sub>Sn<sub>n</sub>I<sub>3n+1</sub> Perovskites. *ACS Energy Lett.* **2017**, *2* (5), 982-990.
50. Ogle, J.; Powell, D.; Amerling, E.; Smilgies, D.-M.; Whittaker-Brooks, L., Quantifying multiple crystallite orientations and crystal heterogeneities in complex thin film materials. *CrystEngComm* **2019**, *21* (38), 5707-5720.
51. Jaeger, A.; Weiser, G.; Wiedemann, P.; Gyuro, I.; Zielinski, E., The sizes of coherent band states in semiconductors, derived from the Franz - Keldysh effect. *J. Phys.: Condens. Matter* **1996**, *8* (36), 6779-6789.
52. Shi, D.; Adinolfi, V.; Comin, R.; Yuan, M.; Alarousu, E.; Buin, A.; Chen, Y.; Hoogland, S.; Rothenberger, A.; Katsiev, K.; Losovyj, Y.; Zhang, X.; Dowben, P. A.; Mohammed, O. F.; Sargent, E. H.; Bakr, O. M., Low trap-state density and long carrier diffusion in organolead trihalide perovskite single crystals. *Science* **2015**, *347* (6221), 519-522.
53. Wu, G.; Li, X.; Zhou, J.; Zhang, J.; Zhang, X.; Leng, X.; Wang, P.; Chen, M.; Zhang, D.; Zhao, K., Fine multi-phase Alignments in 2D perovskite solar cells with efficiency over 17% via slow post-annealing. *Adv. Mater.* **2019**, *31* (42), 1903889.
54. Hansen, K. R.; McClure, C. E.; Colton, J. S.; Whittaker-Brooks, L., Franz-Keldysh and Stark Effects in Two-Dimensional Metal Halide Perovskites. *arXiv preprint arXiv:2109.09021* **2021**.

55. Weiser, G., Stark effect of one-dimensional Wannier excitons in polydiacetylene single crystals. *Phys. Rev. B* **1992**, *45* (24), 14076-14085.
56. Weiser, G.; Horvath, A.; Kolbe, H., Franz-Keldysh effect of band states in polydiacetylene. *Optical Probes of Conjugated Polymers* **1997**, *3145*.
57. Miyata, K.; Zhu, X. Y., Ferroelectric large polarons. *Nat. Mater.* **2018**, *17* (5), 379-381.
58. Khan, M. T.; Shkir, M.; Yahia, I.; Almohammedi, A.; AlFaify, S., An impact of Cr-doping on physical properties of PbI<sub>2</sub> thin films facilely deposited by spin coating technique. *Superlattices Microstruct.* **2020**, *138*, 106370.
59. den Otter, M. W., Approximate expressions for the capacitance and electrostatic potential of interdigitated electrodes. *Sens. Actuators, A* **2002**, *96* (2-3), 140-144.
60. De, A.; Rao, K., Dielectric properties of synthetic quartz crystals. *Journal of materials science* **1988**, *23* (2), 661-664.
61. Muljarov, E. A.; Tikhodeev, S.; Gippius, N.; Ishihara, T., Excitons in self-organized semiconductor/insulator superlattices: PbI-based perovskite compounds. *Phys. Rev. B* **1995**, *51* (20), 14370.
62. Even, J.; Pedesseau, L.; Katan, C., Understanding quantum confinement of charge carriers in layered 2D hybrid perovskites. *ChemPhysChem* **2014**, *15* (17), 3733–3741.
63. Chakraborty, R.; Nag, A., Correlation of dielectric confinement and excitonic binding energy in 2D layered hybrid perovskites using temperature dependent photoluminescence. *J. Phys. Chem. C* **2020**, *124* (29), 16177-16185.
64. Mathieu, H.; Lefebvre, P.; Christol, P., Simple analytical method for calculating exciton binding energies in semiconductor quantum wells. *Phys. Rev. B* **1992**, *46* (7), 4092.
65. Tanaka, K.; Sano, F.; Takahashi, T.; Kondo, T.; Ito, R.; Ema, K., Two-dimensional Wannier excitons in a layered-perovskite-type crystal (C<sub>6</sub>H<sub>13</sub>NH<sub>3</sub>)<sub>2</sub>PbI<sub>4</sub>. *Solid State Commun.* **2002**, *122* (5), 249-252.
66. Wang, Z.; Ganose, Alex M.; Niu, C.; Scanlon, D. O., First-principles insights into tin-based two-dimensional hybrid halide perovskites for photovoltaics. *Journal of Materials Chemistry A* **2018**, *6* (14), 5652-5660.
67. Dyksik, M.; Wang, S.; Paritmongkol, W.; Maude, D. K.; Tisdale, W. A.; Baranowski, M.; Plochocka, P., Tuning the Excitonic Properties of the 2D (PEA)<sub>2</sub>(MA)<sub>n-1</sub>Pb<sub>n</sub>I<sub>3n+1</sub> Perovskite Family via Quantum Confinement. *J. Phys. Chem. Lett.* **2021**, *12* (6), 1638-1643.
68. Stoumpos, C. C.; Cao, D. H.; Clark, D. J.; Young, J.; Rondinelli, J. M.; Jang, J. I.; Hupp, J. T.; Kanatzidis, M. G., Ruddlesden-Popper hybrid lead iodide perovskite 2D homologous semiconductors. *Chem. Mater.* **2016**, *28* (8), 2852-2867.
69. Green, M. A.; Ho-Baillie, A.; Snaith, H. J., The emergence of perovskite solar cells. *Nat. Photonics* **2014**, *8* (7), 506-514.
70. Ziffer, M. E.; Mohammed, J. C.; Ginger, D. S., Electroabsorption Spectroscopy Measurements of the Exciton Binding Energy, Electron-Hole Reduced Effective Mass, and Band Gap in the Perovskite CH<sub>3</sub>NH<sub>3</sub>PbI<sub>3</sub>. *ACS Photonics* **2016**, *3* (6), 1060-1068.
71. Baranowski, M.; Plochocka, P., Excitons in metal-halide perovskites. *Advanced Energy Materials* **2020**, *10* (26), 1903659.
72. Tanaka, K.; Takahashi, T.; Ban, T.; Kondo, T.; Uchida, K.; Miura, N., Comparative study on the excitons in lead-halide-based perovskite-type crystals CH<sub>3</sub>NH<sub>3</sub>PbBr<sub>3</sub> CH<sub>3</sub>NH<sub>3</sub>PbI<sub>3</sub>. *Solid State Commun.* **2003**, *127* (9-10), 619-623.
73. Jeglinski, S. A. Electroabsorption spectroscopy of conjugated polymers and carbon fullerenes and conjugated-polymer light-emitting devices. The University of Utah, 1996.
74. Martin, S. J.; Bradley, D. D. C.; Anderson, H. L., Quadratic Electro-Optic Response of a Conjugated Porphyrin Polymer. *Molecular Crystals and Liquid Crystals Science and Technology. Section A. Molecular Crystals and Liquid Crystals* **1994**, *256* (1), 649-655.
75. Kitazawa, N.; Aono, M.; Watanabe, Y., Temperature-dependent time-resolved photoluminescence of (C<sub>6</sub>H<sub>5</sub>C<sub>2</sub>H<sub>4</sub>NH<sub>3</sub>)<sub>2</sub>PbX<sub>4</sub> (X= Br and I). *Mater. Chem. Phys.* **2012**, *134* (2-3), 875-880.

76. Gupta, S.; Cahen, D.; Hodes, G., How SnF<sub>2</sub> Impacts the Material Properties of Lead-Free Tin Perovskites. *J. Phys. Chem. C* **2018**, *122* (25), 13926-13936.
77. Yin, W.-J.; Yang, J.-H.; Kang, J.; Yan, Y.; Wei, S.-H., Halide perovskite materials for solar cells: a theoretical review. *Journal of Materials Chemistry A* **2015**, *3* (17), 8926-8942.